

Building electronic bursters with the Morris-Lecar neuron model

Alexandre Wagemakers,^{1,*} José M. Casado,² Miguel A. F. Sanjuán,¹ and Kazuyuki Aihara³

¹Nonlinear Dynamics and Chaos Group,

*Departamento de Matemáticas y Física Aplicadas y Ciencias de la Naturaleza,
Universidad Rey Juan Carlos, Tulipán s/n, 28933 Móstoles, Madrid, Spain*

²Area de Física Teórica, Universidad de Sevilla,

Apartado de Correos 1065, 41080 Sevilla, Spain

³Institute of Industrial Science, University of Tokyo, 153-8505, Tokyo, Japan

ERATO Aihara Complexity Modelling Project, JST, 151-0065, Tokyo, Japan

Abstract

We propose a method for the design of electronic bursting neurons, based on a simple conductance neuron model. A burster is a particular class of neuron that displays fast spiking regimes alternating with resting periods. Our method is based on the use of an electronic circuit that implements the well-known Morris-Lecar neuron model. We use this circuit as a tool of analysis to explore some regions of the parameter space and to construct several bifurcation diagrams displaying the basic dynamical features of that system. These bifurcation diagrams provide the initial point for the design and implementation of electronic bursting neurons. By extending the phase space with the introduction of a slow driving current, our method allows to exploit the bistabilities present in the Morris-Lecar system to the building of different models of bursting.

PACS numbers: 05.45.-a, 84.35.+i, 87.10.+e

*Electronic address: alexandre.wagemakers@urjc.es

I. INTRODUCTION

Nowadays the interface between electronic circuits and biological systems is attracting a great deal of research due to the enormous variety of potential applications of electronic devices to the general field of biomedical sciences. Even a connection of an electronic circuit with biological neurons is now possible [1]. As a consequence of this fact, new disciplines such as biomedical engineering or bionics are emerging. From a theoretical viewpoint, the modeling of neurons is becoming more and more accurate, and the electrical behavior of neurons is well reproduced at a quantitative level by the increasingly complex mathematical models that are used in Computational Neuroscience. In this context, the modeling of neurons by means of electronic circuits is a steady growing field that presents rich potentialities for the design of specific hardware that is able to display some useful characteristics for the processing of information in real time.

Experimentation on real neuron is a tough work, the possibility to explore the behaviour of artificial neuron responds to these difficulties. Computational neuroscientists can now dispose of electronic devices as a tool for the exploration in real time of the behaviour of neuron model. Network of artificial neuron can be emulated this way and tested in a real time environment. Connection to in vitro biological neuron forms hybrid networks [2], [3]. The range of medical application of these circuits is prodigious from artificial vision to spinal cord stimulation for hemiplegic patient.

Implementation of neuroelectronic circuit tends to integrate a large number of neuron units in one single chip. The power of integration of electronic devices allows to use complex mathematical models, but the design of the basic units remains a required step before the construction of large array. Despite the power of integration a balance between complexity of the model and the size of circuit should be made. The dynamic should be rich enough to reproduce complex behaviour but the cost of the complexity must be reduced.

In this paper we propose an electronic implementation of a simple model of the giant barnacle motor neuron developed by Morris and Lecar in 1981 [4]. The Morris-Lecar model is a characteristic example of a simple dynamical system presenting a rich and wide variety of dynamical behaviors (see for instance [4] and [5]). It uses only two dynamical variables to describe the state of the neuron and thus allows us a straightforward observation of the phase plane. In fact, with the help of an oscilloscope it is possible to visualize the attractors in real

time. Moreover, depending on the parameters of the model, it presents Hopf (subcritical and supercritical), saddle-node and tangent bifurcations which can be easily observed. By examining these bifurcations as two control parameters are varied we can observe some interesting codimension-2 bifurcations taking place in the system.

We have used an analysis of the Morris-Lecar phase plane to develop a method for the obtention of bursting behavior. Bursters are a class of neurons which are present in many areas of the brain and whose autonomous activity displays periods of fast spiking alternated with resting or silent intervals. Besides, an external current can modulate the bursting response of those neurons and the coupling between bursters can lead to very complex synchronization patterns [6].

The rather complex behavior of a burster is due to coexistence of multiple attractors so that the phase point passes through a succession of different pseudo-attractors as it traces a closed orbit through the phase space. By finding out regions showing bistable behavior in the Morris-Lecar model, we can construct a great variety of bursters. To do that, we take advantage of the hysteretic behavior of the system, leading to paths in the phase plane that are different whether we move a parameter in a way or in the other. In our case the fundamental control parameter will be an external excitatory current delivered to the neuron. By choosing an appropriate dynamics for this current we can allow the system to hop between coexisting states thus giving rise to bursting activity patterns. As examples of our methodology we present a square wave (or fold/homoclinic) burster, an elliptic (sub-Hopf/fold cycle) burster and a cycle/fold burster, all them obtained from the dynamics of the Morris-Lecar neuron model.

II. THE MORRIS-LECAR CIRCUIT

The Morris-Lecar model was originally developed as a mathematical model of the giant barnacle muscle fiber [4]. It pertains to the class of the so-called conductance models and uses a calcium current, a potassium current and a leaky ohmic current to phenomenologically describe the behavior of the nervous fiber. As the dynamics of the calcium channels is much faster than that of the potassium channels, we will consider the former always in the equilibrium state thus reducing the model to the following system of two first order differential equations

$$C \frac{dV_m}{dt} = g_{Ca}^* M_\infty(V_m)(V_m - V_{Ca}) + g_K^* N(V_m - V_K) + g_L(V_m - V_L) + I \quad (1)$$

$$\frac{dN}{dt} = \lambda_N(V_m)(-N + G(V_m)),$$

where V_m is the membrane voltage and N is the activation variable of the slow potassium channels and I is an external tonic current delivered to the neuron. Notice the voltage dependence on V_m of the time constant λ_N in Eqs. (1). We have explicitly

$$\lambda_N(V_m) = \frac{1}{\phi} \cosh((V_m - V_3)/2V_4). \quad (2)$$

On the other hand, g_{Ca}^* and g_K^* are the maximal conductances of the calcium and potassium channels, respectively, and g_L is a constant leak conductance. The conductances of the potassium and calcium channels vary in a sigmoidal way with the membrane voltage V_m . This dependence is introduced by $M_\infty(V)$ and $G(V)$ and is given by the following functions

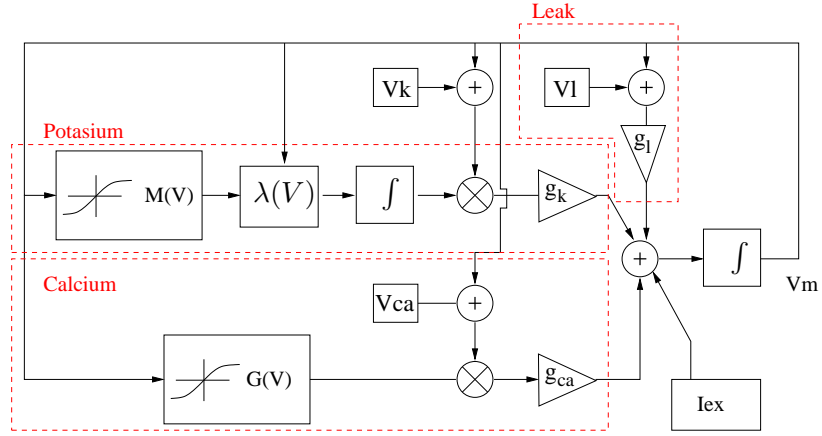
$$M_\infty(V) = 0.5(1 + \tanh((V - V_1)/V_2)), \quad (3)$$

$$G(V) = 0.5(1 + \tanh((V - V_3)/V_4)),$$

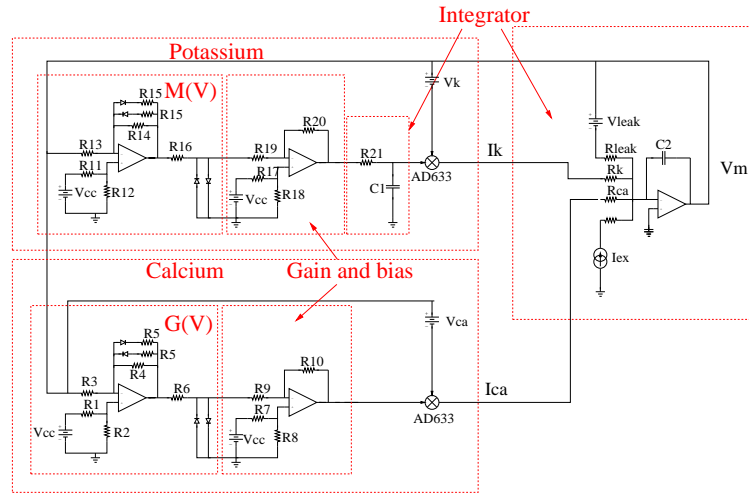
where V_1, V_2, V_3 and V_4 will be considered as adjustable parameters .

As many other mathematical systems describing the electrical activity of the neuron membrane, a strategy based on the use of electronic circuits is well suited to implement its dynamical behavior. The above set of equations can be represented in a block diagram as shown in the Fig. 1.a. This figure represent in a schematic way the equation and will be the basis of the electronic circuit design that is presented in Fig. 1.b. There we can see the three ionic currents which are generated by using the feedback of the voltage membrane V_m into the functional blocks. The calcium current has only one element, the sigmoidal shaped function $G(V)$, whereas the potassium channel include an integrator for the slow dynamics of this channel and also the variable time constant which depends on V_m . That means that the channel does not open and close instantaneously as the calcium channel does, but rather gradually, with a certain inertia. From the viewpoint of the electronics, this means a first order filter. These three currents are summed up and fed into an integrator to generate the membrane voltage.

In order to further reduce the complexity of the model we can make a strong approximation. In the set of Eqs. (1), the differential equation representing the dynamics of the



(a)



(b)

FIG. 1: (a) Block representation of the Morris-Lecar model. We represent the differential equation in “simulink” way, blocks symbolizing integrator transfer functions and multipliers. This logical representation is the basis of the implementation of the circuit. (b) Electronic scheme of the circuit simulating the Morris-Lecar model. The ionic currents are delimited by dashed lines and corresponds to the equivalent blocks in Fig. 1.(a). We suppose the AD633 multiplier correctly biased and adjusted.

potassium channel includes a voltage-dependent time constant $\lambda_N(V_m)$. This parameter results difficult to implement in an electronic circuit. The hard point is to construct a voltage controlled resistor in order to modify the value of the time constant of a RC filter (or first order filter). These components are mainly nonlinear and they introduce noise and undesirable harmonic components. Furthermore, this time constant has a complex influence in the

equation. Nevertheless, when this function is set to a constant, the Morris-Lecar system of equations still exhibits interesting features like a Hopf bifurcation and spiking capabilities. Based on this observation we have reduced the original set of equations to a new set given by

$$C \frac{dV_m}{dt} = g_{Ca}^* M_\infty(V_m)(V_m - V_{Ca}) + g_K^* N(V_m - V_K) + g_L(V_m - V_L) + I, \quad (4)$$

$$\frac{dN}{dt} = \tau^{-1}(-N + G(V_m)),$$

with the same functions $G(V_m)$ and $M_\infty(V_m)$ as in Eq. (3). Here the parameter τ has a *constant* value. This parameter has a critical role in the stability of the system because in the study of fixed points, the Jacobian matrix of the linearized system around the equilibrium point has its eigenvalue depending on the parameter τ .

The proposed circuit is displayed in Fig. 1.b. It uses mainly linear components excepts for the analog multipliers and diodes. With this circuit we can now describe the experiments. The main logical blocks are delimited by dashed lines. The calcium block is made of a sigmoidal function (implemented with pn diodes and an operational amplifier) and an amplifier to adjust the gain and the bias. The output signal is fed into an analog multiplier (AD633) and mixed with the tension V_m . The output of this block is the current I_{Ca} whose expression is

$$I_{Ca} = M_\infty(V_m) \times (V_m - V_{Ca}). \quad (5)$$

The potassium current is quite similar, but now we use an analog integrator (a simple RC circuit). The expression of the ionic current can be described with two equation

$$I_K = N(V_m - V_K), \quad (6)$$

$$\frac{dN}{dt} = \tau^{-1}(-N + G(V_m))$$

The last block, the integrator, sums all the ionic currents and integrate them into a capacitor. The output of this circuit is the membrane voltage V_m . Thus, this variable is the solution of the following differential equation,

$$\frac{dV_m}{dt} = I_K + I_{Ca} + I_L + I, \quad (7)$$

where I_L is a simple ohmic leak. In the next section the equation used by the circuit are slightly different. We have rescaled the output voltage so that the observation of the voltage

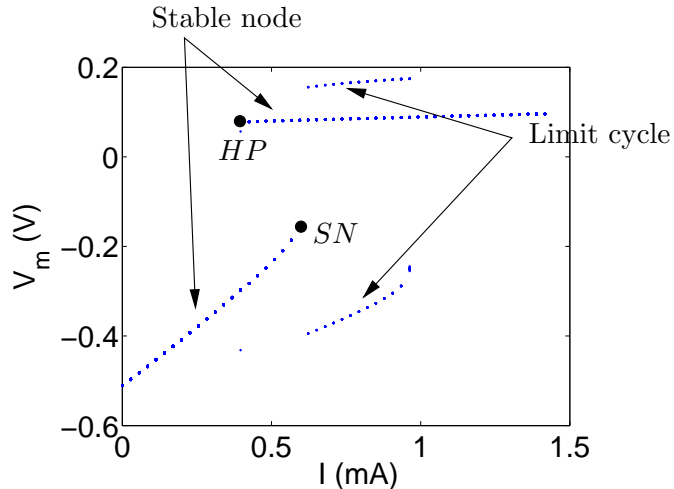


FIG. 2: Experimental bifurcation diagram example in one dimension obtained by plotting the maxima and minima of the membrane voltage V_m as a function of the current I . There we can observe three different attractors: two stable branches, one of them starting from the left and another from the right of the panel, and a stable limit cycle (spiking behavior) coexisting with them between 5 and 10 mA. The bifurcations shown in this diagram are a saddle-node bifurcation on a limit-cycle (SN) and a subcritical Hopf bifurcation (HP).

variable is made much easier. The scaling factor is a non-dimensional number which value is equal to V_{Ca} . The parameters expressed in the following sections are rescaled to this value and so does the membrane voltage. For more details on this normalization see [5]

III. EXPERIMENTAL BIFURCATION DIAGRAMS

The experimental setup for the measurements of the bifurcation diagram is a simple AD/DA converter board. For a fixed set of parameters we construct the bifurcation diagram as a function of a varying external current. We slowly increase the current and observe the changes of the membrane voltage V_m .

In Fig. 2 we plot the maxima and minima of the membrane voltage to visualize the oscillatory behavior and stable states of the system. In this figure there appears a saddle-node bifurcation on an invariant cycle (point SN), a subcritical Hopf bifurcation (point HP) and a limit-cycle (the spiking regime of the neuron). By collecting a great amount of these diagrams in one dimension and joining these one-dimensional diagrams in a bi-parameter

plot we can visualize how the bifurcations in the system evolve when a parameter is moved. Due to the complexity of the whole high dimensional bifurcation diagram, we have limited ourselves to bi-dimensional diagrams with one axis being I and the other being another parameter of the model.

We have chosen three types of bifurcation diagrams which exhibit interesting features: (a) $I - V_3$ plane, where V_3 is the activation threshold of the potassium channel; (b) $I - V_4$ plane, where V_4 is the slope of the activation function for the potassium channel and (c), $I - \tau$ plane, where τ is the time constant of the potassium channel. These parameters have a great influence on the model behavior as we describe below in each case.

A. $I - V_3$ diagram

In the Fig. 3 we show the experimental results obtained by the exploration of the circuit dynamics. We represent the bifurcation with the changes of two parameters I and V_3 . The different attractors and behaviors of the model are specified on the graphics (oscillations and stable node). The bifurcation diagram shows interesting global bifurcations. We observe a Bogdanov-Takens bifurcation (BT point on the panel) and a cusp bifurcation close to it. In fact, these two bifurcations are so close that at the selected scale they cannot be differentiated. The first one represents the transition from a saddle-node bifurcation to a sub-critical Hopf bifurcation, this last bifurcation always lung near a cusp bifurcation. The cusp bifurcation appears when three equilibrium points (a stable one and two unstable) collapse. The change in the excitability of the neuron can be explained considering these bifurcations. As is well known, the Morris-Lecar model is able to support both class I and class II excitabilities. When the parameters are chosen so that class I behavior is displayed, the neuron begins to spike with an almost zero frequency, whereas for type II excitability the spiking begins at nonzero frequency. The change from the type I to type II excitability comes from a Bogdanov-Takens bifurcation which set the transition from a saddle-node bifurcation (type I excitability) to a sub-critical Hopf bifurcation (type II). In our circuit we can control this parameter easily and so we can switch the type of excitability by only changing the parameter V_3 .

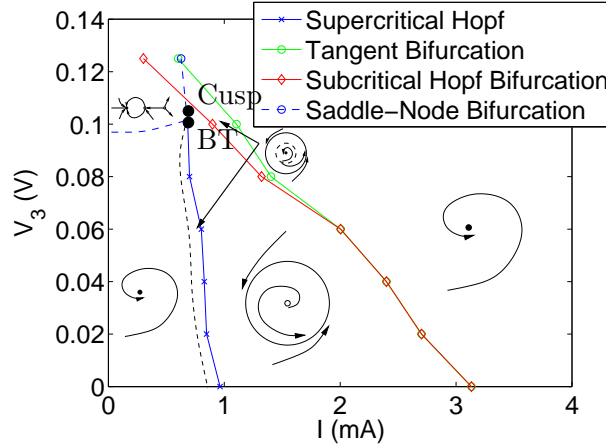


FIG. 3: Codimension-2 bifurcation diagram in the $I - V_3$ plane. We observe a Bogdanov-Takens bifurcation (BT point) and a cusp bifurcation close to it. In this system we have bistable and oscillatory behavior. Stable nodes are displayed with a filled circle and the unstable fixed point with an open circle. Parameter values: $\tau = 0.02$ s, $V_4 = 0.15$ V, $V_2 = 0.15$ V, $V_1 = 0.1$ V, $g_K^* = 8$ mS, $g_{Ca}^* = 4$ mS, $g_L = 2$ mS.

B. $I - V_4$ diagram

This bifurcation diagram in Fig. 4 is quite similar to the previous one in its structure. We observe the same characteristics and the same Bogdanov-Takens and cusp bifurcations (the BT bifurcation always lies near a cusp bifurcation). Besides, a new type of codimension-2 bifurcation appears. This is a generalized Hopf bifurcation (also called a Bautin bifurcation) that corresponds to a transition from a sub-critical to a super-critical Hopf bifurcation [7]. Once again the BT bifurcation changes the excitability of the neuron.

C. $I - \tau$ diagram

The parameter τ is very important for the stability of the system because the dynamics of the potassium current is crucial to the stability of the model. This parameter represents the time of repolarization of the membrane, or in other words, the time necessary for the membrane to return to the resting state after the firing of a spike. In fact, by moving this parameter we can change dramatically the dynamics of the system. The equilibrium

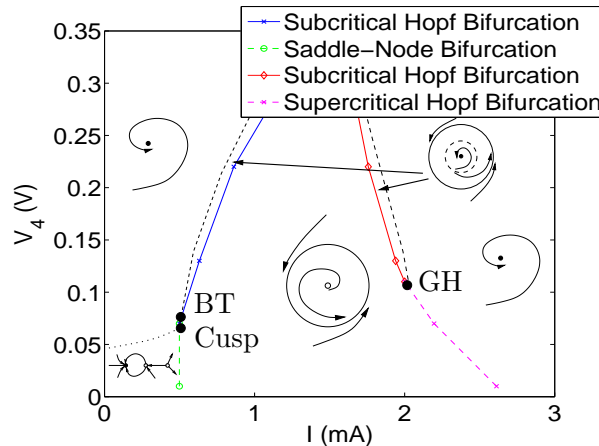


FIG. 4: Codimension-2 bifurcation diagram in the $I - V_4$ plane. A Bogdanov-Takens lies in the plan and a cusp bifurcation is close to it. We found also a generalized Hopf bifurcation which represents the transition from a subcritical to a supercritical Hopf bifurcation. Parameter values: $\tau = 0.02$ s, $V_3 = 0.06$ V, $V_2 = 0.15$ V, $V_1 = 0.1$ V, $g_K^* = 8$ mS, $g_{Ca}^* = 4$ mS, $g_L = 2$ mS.

points remain the same when the parameter τ moves (their positions on the phase plane do not change), but the stability is affected. Figs. 5.a and 5.b show experimental bifurcation diagrams where we observe coexisting bistable and oscillatory regimes. In Fig. 5.a, we have a great zone of bistability. On one side we have the bistability between a stable node and a limit cycle and on the other between two stable nodes (along the line l_1). This particularity can be used for the design of a burster neuron as we will see next.

By modifying the parameter V_4 we obtain the new bifurcation diagram shown in the Fig. 5.b. This diagram displays similar characteristics as the previous one. The saddle-node bifurcation on the limit-cycle is independent of the parameter τ . In this figure we have an interesting bistable zone along the line l_2 where a limit-cycle and a stable node coexist. The transition from one to another occurs through a subcritical Hopf bifurcation and a fold bifurcation. By using this particularity an elliptic burster can be constructed, as it will be described in the next section. Along the line l_3 we have a bifurcation structure identical to the one shown in Fig. 5.a along the line l_1 . On one side a bistability between a limit-cycle and a stable node and on the other between two stable nodes, although the transition from one to another in this case occurs through a saddle-node bifurcation.

The bifurcation diagram appearing in Fig.5.c presents a small bistable zone (the gray

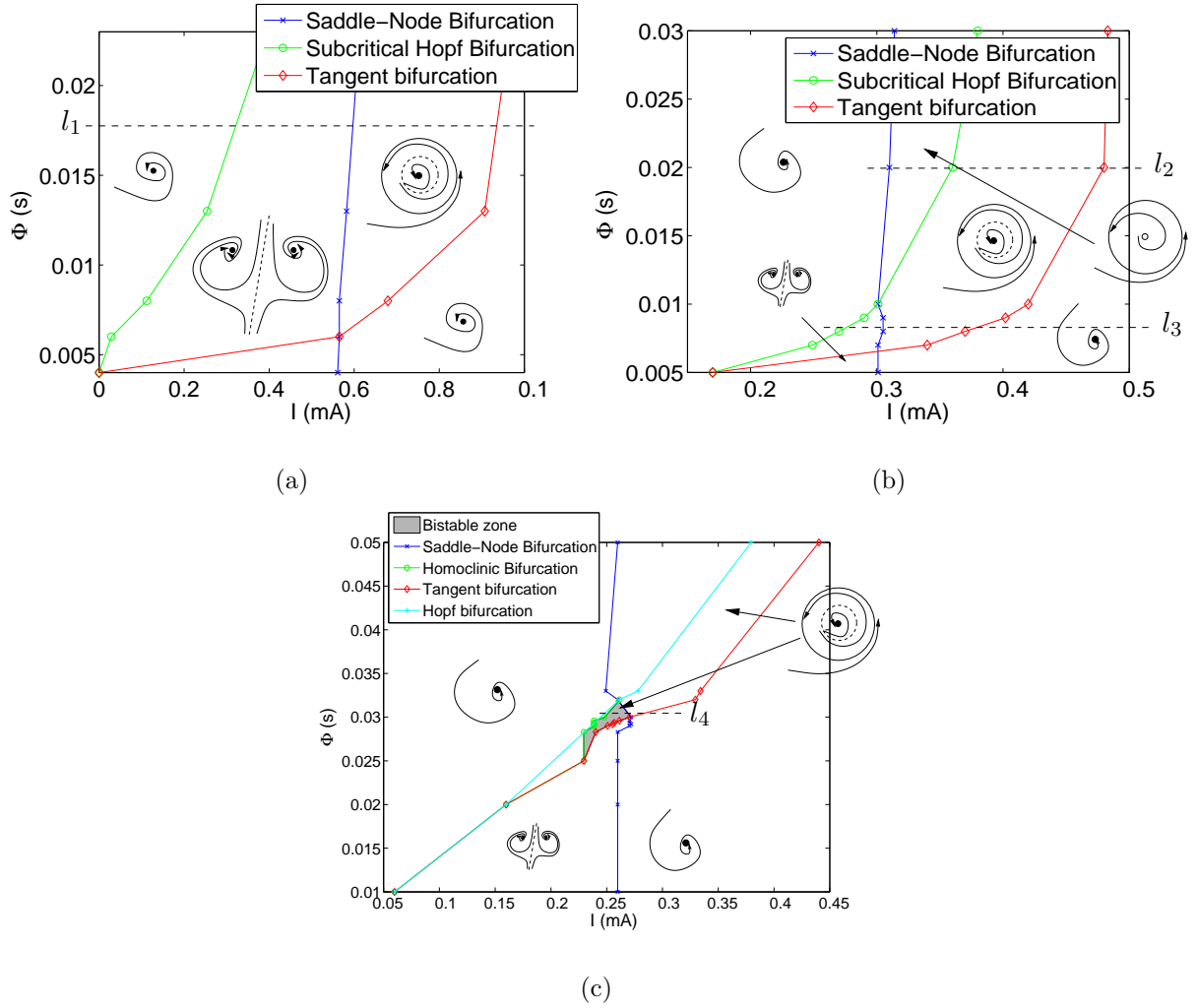


FIG. 5: (a) Codimension-2 bifurcation diagram in the $I - \tau$ plane. We have a large bistable zone represented by the coexistence of a stable node and a limit-cycle (spiking behavior) due to a subcritical Hopf bifurcation. Parameters: $V_4 = 0.07$ V, $V_3 = 0.12$ V, $V_2 = 0.15$ V, $V_1 = 0$, $g_K^* = 8$ mS, $g_{Ca}^* = 4$ mS, $g_L = 2$ mS. (b) In this second figure we changed slightly the parameters of the model and plot anew the bifurcation diagram. This second version is very close from the previous one although small details change. The parameter values are: $V_4 = 0.133$ V, $V_3 = 0.12$ V, $V_2 = 0.15$ V, $V_1 = 0$, $g_K^* = 8$ mS, $g_{Ca}^* = 4$ mS, $g_L = 2$ mS. (c) Detail of the central zone of the bifurcation diagram, where we have a bistable zone between a limit cycle and a stable point. The transition from the limit cycle to the rest state occurs through a homoclinic connection to an unstable point. The parameter values are: $V_4 = 0.07$ V, $V_3 = 0.028$ V, $V_2 = 0.15$ V, $V_1 = -0.032$ V, $g_K^* = 8$ mS, $g_{Ca}^* = 1.38$ mS and $g_L = 2$ mS.

shaded zone) where a stable node and a limit cycle coexist. If the system is on the stable node, when we increase the external current the attractor changes to a spiking regime after a saddle-node bifurcation. On the other hand, when the current decreases the stable limit cycle collapses with an unstable fixed point. Although this region of bistability always remains in a narrow range of parameters it can be a good candidate for the design of the square wave burster.

IV. THE DESIGN OF BURSTERS

The previous experiments are the basis for the implementation of some models of bursting behavior. Since a burster works by switching between two (pseudo-)stable attractors (a limit-cycle and a stable node for example), we have to spot the bistable zones of the parameter space. Here the previous experimental work is essential, since we can visually find out the bistable regimes of the neuron model. So, the first step is the search for bistable states where we can switch easily from one attractor to another by simply varying the external current. In the previous diagrams we have to look for a bistable regime along a horizontal line. For example, following the line l_2 in Fig. 5.b we have a bistable behavior between a stable node and a stable limit-cycle. When the external current is moved a hysteresis loop appears between the rest state and the spiking state (Fig. 6). This hysteresis loop leads to transitions from the resting state to the spiking regime and back. Once we have chosen two coexisting states as good candidates for the switching we introduce a new differential equation in our system to allow this switching to take place. This new equation governs the slow current I , and is given by the expression

$$R_b \frac{dI}{dt} = \frac{1}{RC}(V_m - V_{th}), \quad RC \gg \tau. \quad (8)$$

The introduction of the new variable $I(t)$ allows us to switch the whole dynamics from one attracting state to another by a suitable election of values of R_b and V_{th} . Observe that now I is really an “internal” variable of the extended dynamical system. The equation (8) is implemented by using a simple operational amplifier in integrator mode. In order to develop our method, we start by marking the interesting bistable zone on the bifurcation diagram (horizontal line l_1 on Fig. 5) and extracting the corresponding projection in one dimension (current vs amplitude on Fig. 2). Setting the voltage threshold V_{th} in Eq. 8 is a rather

difficult task because the integrate current must decrease when the burster is spiking and must increase when the burster is in its resting state. The resulting waveform of this current for the square-wave burster is shown in Fig. 7. Notice that the current I is increasing when $\langle V_m \rangle$ (where $\langle \cdot \rangle$ holds for the mean value) is above the threshold and decreasing when it is below V_{th} . The second parameter R_b is important for the strength of the feedback current in the circuit.

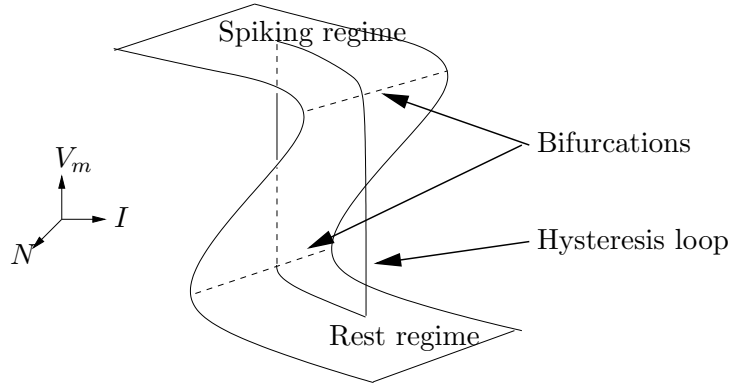


FIG. 6: Hysteresis loop of the burster. Observe that the system switches from a rest state to a spiking regime and back when the current I is changed.

A. Square wave burster (“Fold/homoclinic” burster)

First, we have built the well-known square-wave (or fold/homoclinic) burster ([8],[9]). This burster displays oscillations between a stable limit cycle and a stable node. In Fig. 5.c we have found a small region of bistability between an oscillatory state with an homoclinic connection and a stable node. This small region is shaded in grey. If we sketch the behavior of V_m along the line l_4 drawn in Fig. 5.c, a graph similar to the one displayed in Fig.7.c is obtained. The bistable regime can be seen on the bifurcation diagram appearing in Fig. 7.c. Although this bistable regime only occurs in a narrow range of I we can apply the technique to this case. Here the transition between the two states takes place through a fold bifurcation for the passage from the resting point to spiking activity and through an homoclinic connection of the unstable node for the transition from activity to rest).

In Fig. 7.b we have an example of bursting oscillation between two attractors in the three dimensional phase space. We also plot the corresponding time series of the voltage in Fig.

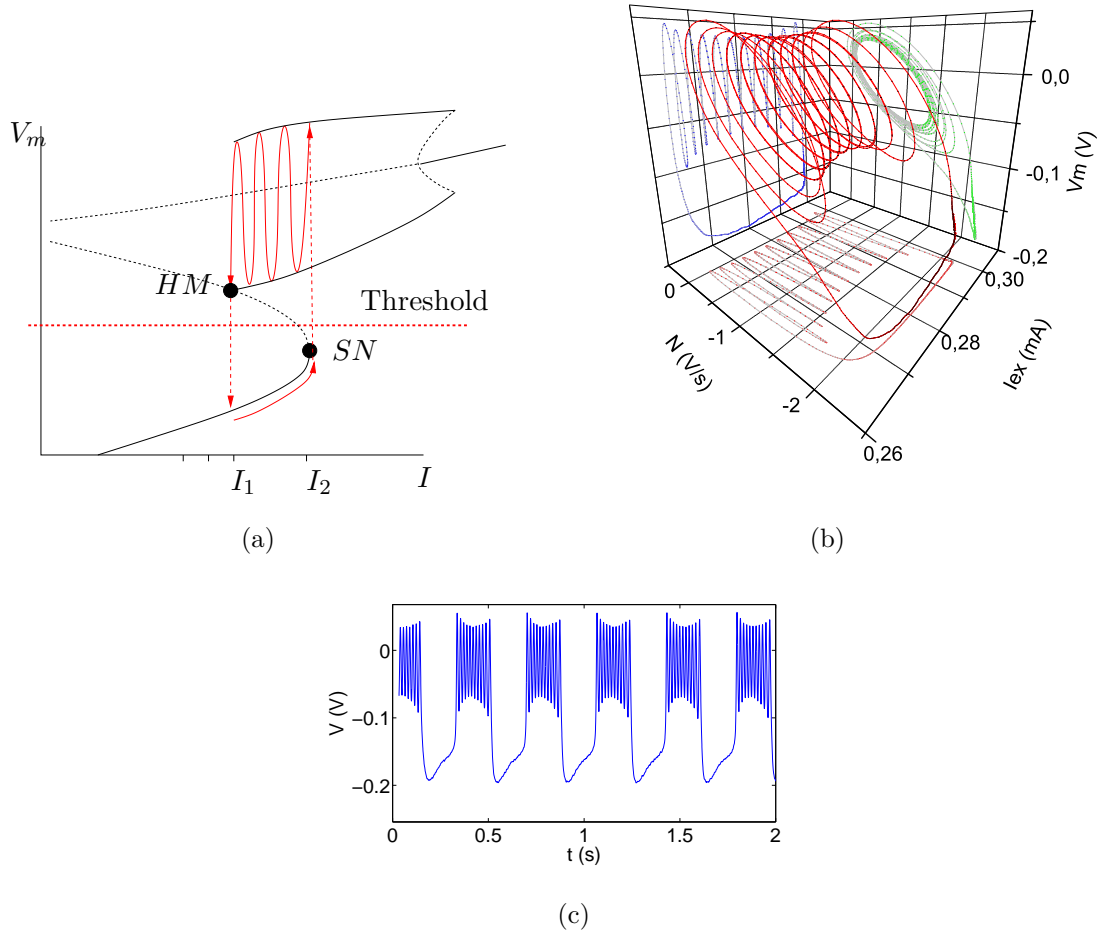


FIG. 7: (a) Dynamical principle of the square-wave burster. The figure represents the bifurcation diagram of the Morris-Lecar model as a function of I . The bursting regime appears through a fold bifurcation for the passage from the stable node to the limit cycle and through a homoclinic connection when the cycle loses its stability and gets back to the rest state; (b) 3D view of the orbit in the space (I, N, V_m) . The parameter values are: $\tau = 0.03$ s, $V_4 = 0.07$ V, $V_3 = 0.028$ V, $V_2 = 0.15$ V, $V_1 = -0.032$ V, $g_K^* = 8$ mS, $g_{Ca}^* = 1.38$ mS, $g_L = 2$ mS, $R_s = 4.3$ k Ω , $R_b = 13.7$ k Ω . (c) Time series of the membrane voltage corresponding to the output of the circuit.

7.c, where the temporal characteristics of the bursting are evident.

B. Elliptic burster (“subHopf/fold cycle” burster)

We have simulated also the elliptic burster. Once again the bistability is the key point. But in this case the nature of the bifurcation is totally different. In Fig. 8.b we have a representation of the oscillation in the full three dimensional phase space. The solid red line corresponds to the trajectory in phase space. The transition from the resting to the spiking regime takes place through a subcritical Hopf bifurcation and the reverse transition occurs through the tangent bifurcation (the unstable limit cycle collapses with the stable cycle, (this bifurcation is also called a “fold cycle”). This kind of behavior can be seen along the line l_2 in the figure 5.b, where we can see a bistable region due to the sub-critical Hopf bifurcation. We can configure the system to oscillate along the line l_2 .

In Fig. 8.b we represent the experimental phase space, a three dimensional space spanned by the membrane voltage, the current and the potassium channel activation. In Fig. 8.c we have plotted the time series of the voltage V_m . The Fig. 8.d depicts the variation of the excitation current.

C. “circle/fold cycle” burster

This kind of burster is quite close from the previous one but the bifurcation have a different nature. There are three different transitions. On the bifurcation diagram in Fig. 5.b we drawn the line l_3 . Along this line we have some different bistable states like two stable nodes, a stable node and a stable limit cycle.

The bursting starts after a saddle-node bifurcation on a limit-cycle. The current goes increasing till the tangent bifurcation (the fold/cycle bifurcation) takes place and then the system gets back to a new stable node. The current is now decreasing and reduce until the sub-critical Hopf bifurcation occurs. Once this bifurcation is passed the system returns to the first stable state and the cycle starts over. We summarize this complex behavior in Fig. 9 where we can see clearly how the sequence of attractors is followed by the dynamical system. In panel (a) we have plotted a schematic view of the phase space. In (b) a view of the experimental attractor in the three-dimensional phase space is depicted. The panel (c) shows the temporal evolution of the membrane voltage as the system carries out some cycles of bursting.

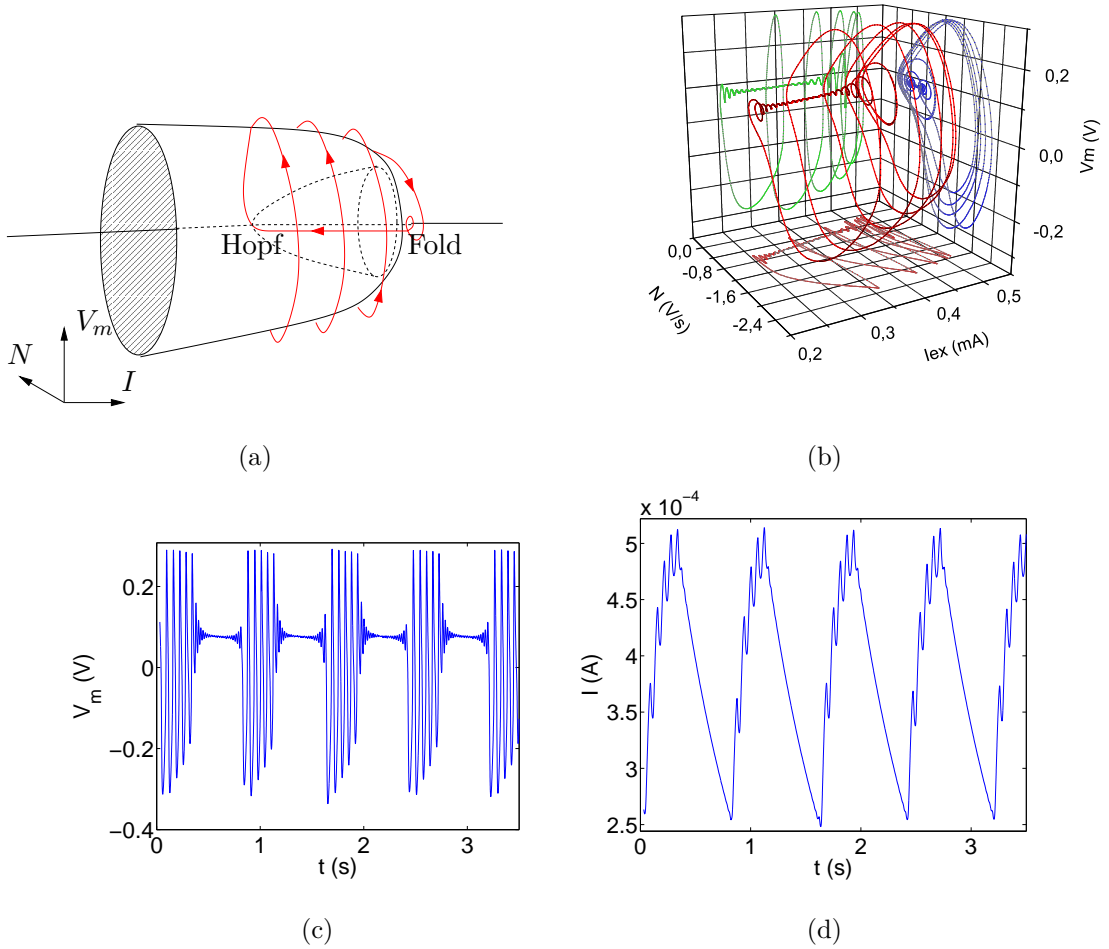


FIG. 8: (a) Bursting principle of the elliptic burster. The bursting is done through a sub-critical Hopf bifurcation. The gray shade represent the limit cycle and the solid line the stable state. (b) View of the phase space of the system, the variables are (V_m, N, I) , parameters: $\tau = 0.079$ s, $V_4 = 0.07$ V, $V_3 = 0.12$ V, $V_2 = 0.15$ V, $V_1 = 0$, $g_K^* = 8$ mS, $g_{Ca}^* = 4$ mS, $g_L = 2$ mS, $R_8 = 174$ k Ω , $R_b = 10$ k Ω . (c) Time series generated by an elliptic burster built from the Morris-Lecar circuit. Observe the growing of the oscillation as the sub-critical Hopf bifurcation is approached. (d) Time series of the current I .

V. CONCLUSIONS

We have designed and built a circuit that approximates the main dynamical regimes of the well-known Morris-Lecar neuron model. By analyzing the behavior of this system in the phase space in terms of some of the parameters of the model we have been able to obtain

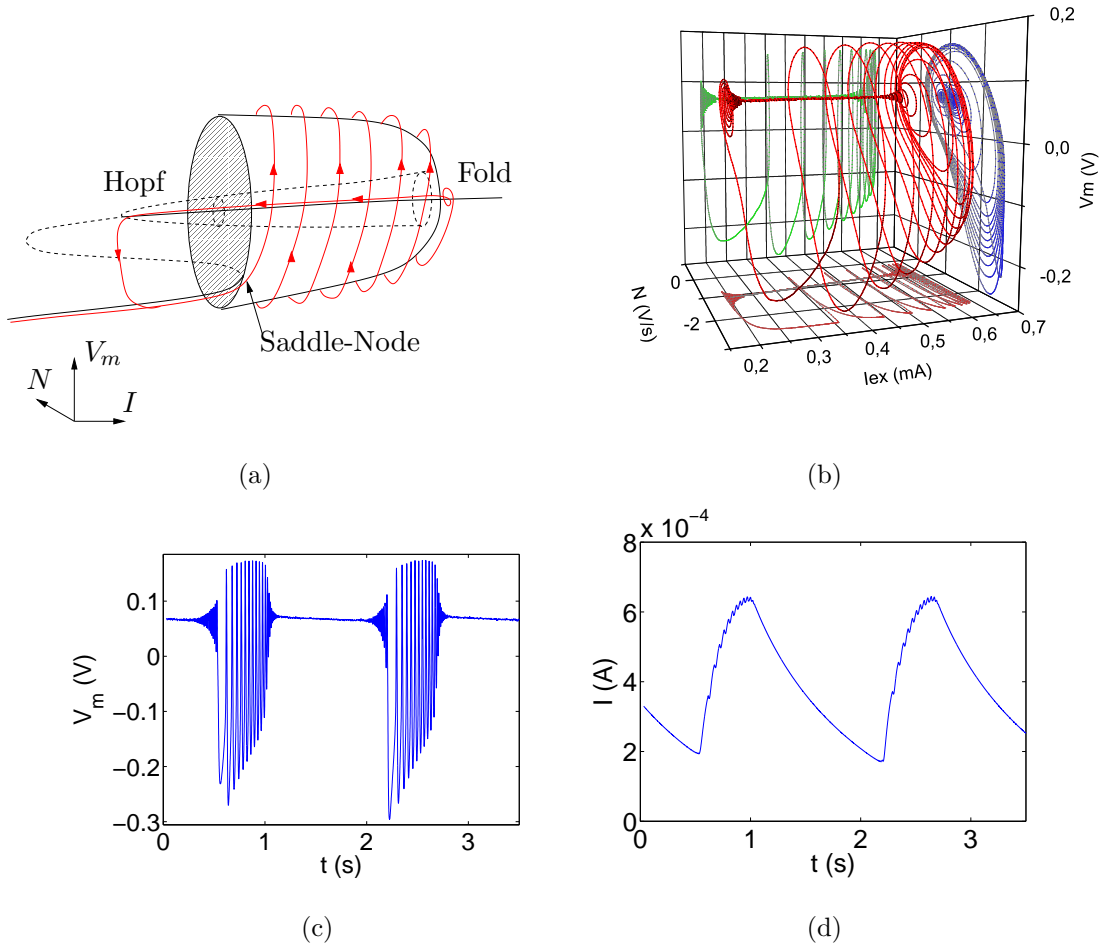


FIG. 9: (a) Dynamical principle of the circle/fold burster. The transition from rest to the oscillatory state is made through a saddle-node bifurcation on a limit-cycle. The cycle collapse with a fold bifurcation and the system remains on a stable state until it returns to the original trough a subcritical Hopf bifurcation. (b) Experimental measurement of the attractor, view in the three-dimensional phase space (V_m, N, I). The parameter values are $\tau = 0.026$ s, $V_4 = 0.07$ V, $V_3 = 0.12$ V, $V_2 = 0.15$ V, $V_1 = 0$, $g_K^* = 8$ mS, $g_{Ca}^* = 4$ mS, $g_L = 2$ mS, $R_8 = 4.3$ k Ω , $R_b = 10$ k Ω (c) Time series of the V_m variable. (d) Time series of the current I

different bursting behaviors each one of them characterized by the visiting of a particular succession of attractors of the whole system by the evolving phase point. Thus, our strategy provides a method to investigate the features of relatively simple dynamical systems giving rise to rather complex cycles in the phase space that appear as the phase point transiently

visits a given set of the stable attractors of the whole dynamical system.

The implementation of the method by means of an electronic circuit introduces a great flexibility in the real time control of the characteristics of the system. In particular, this method allow us to carry out a continuous control of the behavior of the system by allowing the continuous observation of the system's output as the parameters are changed. The use of electronics circuits is an advantage in this context because they are physical devices that operate in a real environment and thus they are subject to a great deal of uncontrollable noise. This is in fact the environment in which evolve real dynamical systems as neurons and so, our method could provide an approach to analyze the robustness of the dynamics of neuronal models under real world situations.

Acknowledgments

This work has been supported by the Spanish Ministry of Science and Technology under project number BFM2003-03081. A financial aid from the Universidad Rey Juan Carlos for a research stay in the University of Tokyo, where part of this work was carried out is also acknowledged.

VI. PARAMETERS USED IN THE EXPERIMENT

Parameter	Values	Units
Φ	$R_{21} \times C_1$	s
V_1	$-V_{cc} \times R_1 / (R_1 + R_1)$	V
V_2	$-R_3 / R_4$	V
V_3	$-V_{cc} \times R_{11} / (R_{11} + R_{12})$	V
V_4	$-R_{13} / R_{14}$	V
g_{Ca}^*	$1 / R_{Ca}$	S
g_K^*	$1 / R_K$	S
g_L	$1 / R_L$	S
OPAMP	UA741	–
V_{cc}	10	V
Mutiplier	AD633	–

-
- [1] S. L. Masson, A. Laflaquiere, T. Bal, and G. L. Masson, *IEEE Transaction on Biomedical Engineering* **46**, 638 (1999).
- [2] G. Zeck and P. Fromherz, *PNAS* **98**, 10457 (2001).
- [3] M. F. Simoni, G. S. Cymbalyuk, M. E. Sorensen, R. L. Calabrese, and S. P. DeWeerth, *Biomedical Engineering, IEEE Transactions on*, Iss.2 **51**, 342 (2004).
- [4] C. Morris and H. Lecar, *Biophys. J.* **35**, 193 (1981).
- [5] J. Rinzel and B. Ermentrout, in *C. Koch and I. Segev, editors, Methods in Neuronal Modeling* (MIT press, 1989), pp. 135–169.
- [6] J. M. Casado, B. Ibarz, and M. A. F. Sanjuán, *Modern Physics Letters B* **18**, 1347 (2004).
- [7] Y. A. Kuznetsov, *Elements of applied bifurcation theory* (Springer, 1998).
- [8] H. Wilson, *Spikes, decisions, and actions* (Oxford University Press, 1999).
- [9] F. Hoppensteadt and E. Izhikevich, *Analysis of neural excitability and oscillations* (Springer, 1997).